Available online at www.sciencedirect.com
SCIENCE DIRECT®
Journal of Sound and Vibration 278 (2004) 343–363
JOURNAL OF SOUND AND VIBRATION
www.elsevier.com/locate/jsvi

The finite element analysis and experimental study of beams with active constrained layer damping treatments

Yinming Shi[a,b,*], Hongxing Hua[a], Hugo Sol[b]

[a] *The National Key Laboratory for Vibration, Shock & Noise, Shanghai Jiaotong University, 200030 Shanghai, People's Republic of China*

[b] *Department Mechanics of Materials and Constructions (MEMC), Faculty of Applied Science, Vrije Universiteit Brussels, Building KB, Pleinlaan 2, B-1050 Brussels, Belgium*

Received 10 February 2003; accepted 7 October 2003

Abstract

Vibration control of structures is confronted with many problems like the proper selection of modelling methods, controllability and observability of models, model size and model reduction methods. In this paper a practical procedure is proposed to overcome technical problems of structure control due to a large model size. Firstly, an accurate numerical model is derived by using the finite element method. This model is verified by modal analysis experiments. Secondly, a new model reduction procedure is proposed to reduce considerably the full order model. This reduction makes the reduced order model controllable and observable. In a further step, a controller is designed based on the verified reduced order model. Finally, a real-time control system is set up. The controlled and uncontrolled impulse responses at the free tip of the cantilever beam with active constrained layer damping treatments are compared both in time domain and frequency domain. The results clearly show the efficiency of the proposed procedure. The procedure proposed in this paper can be extended towards more complex structures.

1. Introduction

Conventional passive constrained layer damping (PCLD) is obtained by putting a layer of viscoelastic material (VEM) between the base structure and a constraining layer. The passive damping energy is generated mainly by shear stresses in the viscoelastic layer. PCLD treatments [1–3] have been applied to machines and structures widely over the last century because of their reliability and simplicity. PCLD treatments can reduce vibrations effectively at high-frequency

*Corresponding author. Fax: 0032-2-629-2928.
E-mail address: shiyinming@hotmail.com, yinming.shi@vub.ac.be (Y. Shi).

0022-460X/$ - see front matter © 2003 Elsevier Ltd. All rights reserved.
doi:10.1016/j.jsv.2003.10.009

ranges, but they are not so effective at low-frequency ranges. Furthermore, they are not intelligent and once the damping treatments are installed, they cannot be adjusted and cannot adapt themselves to changeable environments. Structure damping can also be obtained in an active way by fixing a piezoelectric (PZT) layer directly on the base structure. Extension and compression of the PZT layer can be controlled by an electrical voltage signal. Recently, active damping has received increased attention in the aeronautic and astronautic industries, owing to the significant and adjustable damping it can offer. Yet in spite of productive research into active damping treatments [4–6], many limitations remain. Safety and reliability cannot be guaranteed. Active damping is effective in the low-frequency range, but is difficult to implement at high-frequency ranges. Hybrid damping is a combination of PCLD with active damping treatments. To obtain hybrid damping, active constrained layer damping (ACLD) treatments [7,8] in which the constraining layer of PCLD treatments is replaced by a PZT layer have been proposed. Hybrid damping hence combines the efficiency of PCLD in the high-frequency range with the efficiency of active damping in the low-frequency range.

The main difficulties with hybrid damping are that the active controller is very sensitive to system changes and the VEM properties change with frequency and temperature. Hence in order to design a reasonable, sufficiently reliable and robust control system, both the VEM and the host structure must be well modelled.

Many models have been used to deal with VEM. The simplest model is the complex modulus model $E^* = (E' + \mathrm{i}E'')$ with constant real E' and constant imaginary E'' values. Rongong and Wright [9], Baz [10], Shen [11], Baz and Ro [12] used this model to study ACLD. The advantage of the complex modulus model is its simplicity; the drawback is that it can only describe the dynamical properties correctly when the applied load is harmonic [13]. Another popular model for VEM is the iterative modal strain energy (MSE) model. Veley and Rao [14] used this model. The advantage of the MSE model is that researchers need only to solve the real eigenvalue problem instead of the complex eigenvalue problem. However, this will result in unacceptable errors for the calculated damping factors if the natural frequencies are not well separated [15]. The fractional derivative (FD) model is another model adopted to study VEM. The FD model is exact enough to describe the dynamic properties of VEM, but it results in high-order equations and is not convenient to calculate the response in the time domain [13]. Another model proposed to study VEM is the anelastic displacement fields (ADF) model [16]. The ADF model introduces extra degrees of freedom (d.o.f.'s) and results in a first order linear system. Lesieutre and Lee [17] used the ADF model to study an ACLD system. Similar to ADF, the Golla–Hughes–McTavish (GHM) [18,19] model introduces extra d.o.f.'s, but here this results in traditional second order equations in the time domain. Many researchers employed the GHM model to study ACLD systems, e.g., Margaretha [20], Liao and Wang [21,22], Shi [23]. The advantage of GHM is its complete compatibility with the finite element method (FEM). This means all useful and mature features of the FEM can be retained.

ACLD structures are either modelled by the FEM or by distributed parameter method (DPM) based on analytical equations. Rongong and Wright [9] used a DPM to study the axial and transverse vibrations of a beam. They applied a Ritz method to derive the eigenfrequencies. Based on an eight order differential equation, Shen [11] studied the controllability, observability and stability of an ACLD beam system. Baz [24] proposed a stable boundary control strategy based on analytical equations. Baz [25] numerically studied different control strategies based on

analytical equations. All the models derived from DPM are small and exact enough, but unfortunately DPM is limited only to simple structures such as ACLD beam structures. Since the GHM model is completely compatible with the FEM, which is a powerful alternative used to model ACLD structures. Van Nostrand [26] studied the transverse vibration of an ACLD beam using finite elements derived with the Euler–Bernoulli theory. Veley and Rao studied ACLD structures modelled with finite elements and the MSE model for the viscoelastic material. Friswell and Inman [27] studied a PCLD beam using the FEM and the GHM model for the viscoelastic material. They discussed a possible model reduction for the studied PCLD system. Shi [23] used the FEM and the GHM model to study ACLD structures. Many research activities are limited to numerical simulation because of the uncontrollability and unobservability of ACLD structures. Zehn [28] proposed a practical way to investigate ACLD structures based on a commercial FE software COSAR, a commercial controller design software MATLAB/SIMULINK and a commercial modal analysis equipment of LMS.

This paper proposes an alternative and practical way to attenuate the vibration of structures. A combined finite element analysis and an experimental study of a cantilever beam with a hybrid damping treatment are presented. A viscoelastic layer is fixed on the beam with a PZT constraining layer to obtain a hybrid damping. A GHM model is used to describe the frequency-dependant behavior of the shear modulus. The cantilever beam with ACLD treatment is modelled with FEM. The FE model is validated by modal experiments. Next, a new model reduction procedure is proposed. The reduced model is much smaller in d.o.f. and is observable and controllable. The paper describes further how a suitable damping controller is designed. Real-time vibration control experiments are performed to validate the described procedure. The experimental results clearly show the obtained damping performance of the controlled hybrid system.

2. Analysis based on a finite element model

Fig. 1 shows a cantilever base beam partially covered ACLD consisting of a PZT layer on top of a VEM layer. A FE model will be developed based on those assumptions: (1) The rotary inertia is negligible. Shear deformations in the PZT and the base beam are negligible. (2) The transverse displacement w is the same for all three layers. (3) Young's modulus of the VEM is negligible as compared to those of the beam and PZT materials. (4) Linear theories of elasticity, viscoelasticity, and piezoelectricity are used. (5) There is perfect continuity at the interface and no slip occurs between the layers. (6) The applied voltage is uniform along the PZT. (7) Density and thickness are uniform over the beam.

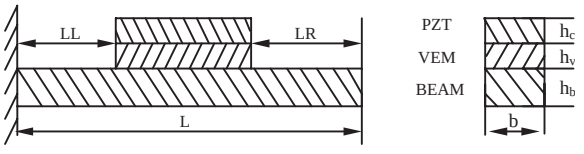

Fig. 1. Cantilever beam partially covered with an ACLD layer.

2.1. Finite element modelling

The FE-model for the cantilever beam, partially covered with an ACLD, is divided into special purpose ACLD elements and normal Euler–Bernouilli beam elements.

2.1.1. ACLD elements

Fig. 2 shows a two nodes ACLD element. The nodal displacements are given by

$$\{U^{(e)}\} = [w_i^{(e)}\ \theta_i^{(e)}\ u_{ci}^{(e)}\ u_{bi}^{(e)}\ w_j^{(e)}\ \theta_j^{(e)}\ u_{cj}^{(e)}\ u_{bj}^{(e)}]^{\mathrm{T}}. \tag{1}$$

The transverse and the axial displacements of the base beam, and the axial displacement of the PZT are expressed in the nodal displacements by shape functions:

$$w = [N_w]\{U^{(e)}\}, \quad \theta = [N_w]'\{U^{(e)}\}, \quad u_c = [N_c]\{U^{(e)}\}, \quad u_b = [N_b]\{U^{(e)}\}, \tag{2}$$

where

$$\begin{aligned}[N_w] &= [1-3\xi^2+2\xi^3\ \ (\xi-2\xi^2+\xi^3)L_e\ 0\ 0\ 3\xi^2-2\xi^3\ \ (-\xi^2+\xi^3)L_e\ 0\ 0],\\ [N_c] &= [0\ 0\ 1-\xi\ 0\ 0\ 0\ \xi\ 0], \quad [N_b] = [0\ 0\ 0\ 1-\xi\ 0\ 0\ 0\ \xi],\end{aligned} \tag{3}$$

$\xi = x/L_e$ is the local element co-ordinate.

From the kinematic relationships between the PZT layer and the base beam, it is easy to derive the following relations [29]:

$$\begin{aligned}u_v &= \frac{u_c+u_b}{2} + \frac{(h_c-h_b)}{4}\frac{\partial w}{\partial x},\\ \gamma &= \frac{u_c-u_b}{h_v} + \frac{\partial w}{\partial x}\left(\frac{h_c+h_b+2h_v}{2h_v}\right),\end{aligned} \tag{4}$$

γ and u_v can also be expressed as functions of the nodal displacements by finite element shape functions:

$$u_v = [N_v]\{U^{(e)}\}, \quad \gamma = [N_\gamma]\{U^{(e)}\}, \tag{5}$$

with

$$[N_v] = \frac{1}{2}([N_c]+[N_b]) + \frac{h_c-h_b}{4}[N_w]',$$

$$[N_\gamma] = \frac{1}{h_v}\left[-\frac{6h^*}{L_e}\xi + \frac{6h^*}{L_e}\xi^2\ \ h^*(1-4\xi+3\xi^2)\ \ 1-\xi\ \ \xi-1\ \ \frac{6h^*}{L_e}\xi - \frac{6h^*}{L_e}\xi^2\ \ h^*(-2\xi+3\xi^2)\ \ \xi\ \ -\xi\right],$$

$$h^* = (h_c-h_b)/4.$$

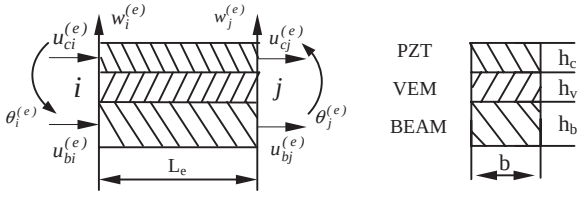

Fig. 2. An ACLD element.

For the base beam layer of an ACLD element, the potential and the kinetic energy are

$$\begin{aligned}
&\frac{1}{2}\int_0^{L_e} E_b b h_b \left(\frac{\partial u_b}{\partial x}\right)^2 \mathrm{d}x + \frac{1}{2}\int_0^{L_e} E_b I_b \left(\frac{\partial^2 w}{\partial x^2}\right)^2 \mathrm{d}x \\
&\quad = \frac{1}{2}\{U^{(e)}\}^{\mathrm{T}}[K_{bu}^{(e)}]\{U^{(e)}\} + \frac{1}{2}\{U^{(e)}\}^{\mathrm{T}}[K_{bw}^{(e)}]\{U^{(e)}\}, \\
&\frac{1}{2}\int_0^{L_e} \rho_b h_b b \left(\frac{\partial u_b}{\partial t}\right)^2 \mathrm{d}x + \frac{1}{2}\int_0^{L_e} \rho_b h_b b \left(\frac{\partial w}{\partial t}\right)^2 \mathrm{d}x \\
&\quad = \frac{1}{2}\{\dot{U}^{(e)}\}^{\mathrm{T}}[M_{bu}^{(e)}]\{\dot{U}^{(e)}\} + \frac{1}{2}\{\dot{U}^{(e)}\}^{\mathrm{T}}[M_{bw}^{(e)}]\{\dot{U}^{(e)}\},
\end{aligned} \tag{6}$$

where

$$[K_{bu}^{(e)}] = E_b b h_b L_e \int_0^1 [N_b]'^{\mathrm{T}}[N_b]' \,\mathrm{d}\xi, \quad [K_{bw}^{(e)}] = E_b I_b L_e \int_0^1 [N_w]''^{\mathrm{T}}[N_w]'' \,\mathrm{d}\xi,$$

$$[M_{bu}^{(e)}] = \rho_b h_b b L_e \int_0^1 [N_b]^{\mathrm{T}}[N_b] \,\mathrm{d}\xi, \quad [M_{bw}^{(e)}] = \rho_b h_b b L_e \int_0^1 [N_w]^{\mathrm{T}}[N_w] \,\mathrm{d}\xi.$$

For the PZT layer of an ACLD element, the constitutive equations of PZT materials for one-dimensional structures with uni-axial loading can be written as [4]

$$\begin{bmatrix} \varepsilon \\ D \end{bmatrix} = \begin{bmatrix} S_{11}^E & d_{31} \\ d_{31} & \varepsilon_{33}^{\tau} \end{bmatrix} \begin{bmatrix} \tau \\ E \end{bmatrix}, \tag{7}$$

the potential and the kinetic energy of the PZT layer are

$$\begin{aligned}
&\frac{1}{2}\int_0^{L_e} E_c b h_c \left(\frac{\partial u_c}{\partial x}\right)^2 \mathrm{d}x + \frac{1}{2}\int_0^{L_e} E_c I_c \left(\frac{\partial^2 w}{\partial x^2}\right)^2 \mathrm{d}x \\
&\quad = \frac{1}{2}\{U^{(e)}\}^{\mathrm{T}}[K_{cu}^{(e)}]\{U^{(e)}\} + \frac{1}{2}\{U^{(e)}\}^{\mathrm{T}}[K_{cw}^{(e)}]\{U^{(e)}\}, \\
&\frac{1}{2}\int_0^{L_e} \rho_c h_c b \left(\frac{\partial u_c}{\partial t}\right)^2 \mathrm{d}x + \frac{1}{2}\int_0^{L_e} \rho_c h_c b \left(\frac{\partial w}{\partial t}\right)^2 \mathrm{d}x \\
&\quad = \frac{1}{2}\{\dot{U}^{(e)}\}^{\mathrm{T}}[M_{cu}^{(e)}]\{\dot{U}^{(e)}\} + \frac{1}{2}\{\dot{U}^{(e)}\}^{\mathrm{T}}[M_{cw}^{(e)}]\{\dot{U}^{(e)}\},
\end{aligned} \tag{8}$$

where

$$[K_{cu}^{(e)}] = E_c b h_c L_e \int_0^1 [N_c]'^{\mathrm{T}}[N_c]' \,\mathrm{d}\xi, \quad [K_{cw}^{(e)}] = E_c I_c L_e \int_0^1 [N_w]''^{\mathrm{T}}[N_w]'' \,\mathrm{d}\xi,$$

$$[M_{cu}^{(e)}] = \rho_c h_c b L_e \int_0^1 [N_c]^{\mathrm{T}}[N_c] \,\mathrm{d}\xi, [M_{cw}^{(e)}] = \rho_c h_c b L_e \int_0^1 [N_w]^{\mathrm{T}}[N_w] \,\mathrm{d}\xi.$$

If a virtual displacement field is applied, the virtual work done by the induced virtual strain in the PZT layer is

$$\delta w_c = \int_0^{L_e} E_c d_{31} b v(t) \delta\left(\frac{\partial u_c}{\partial x}\right) \mathrm{d}x = [\delta U^{(e)}]^{\mathrm{T}} \{f_c^{(e)}\} \tag{9}$$

with the induced strain force in the element nodes

$$\{f_c^{(e)}\} = E_c d_{31} b v(t) [0 \ 0 \ -1 \ 0 \ 0 \ 0 \ 1 \ 0]^{\mathrm{T}}.$$

A GHM-model is adopted to model the VEM layer in an ACLD element. The GHM model represents the shear modulus as a series of mini-oscillator terms in the Laplace domain [19]:

$$s\tilde{G}(s) = G^{\infty}\left[1 + \sum_{k=1}^{N} \alpha_k \frac{s^2 + 2\hat{\zeta}_k \hat{\omega}_k s}{s^2 + 2\hat{\zeta}_k \hat{\omega}_k s + \hat{\omega}_k^2}\right]. \tag{10}$$

The positive constants α_k, $\hat{\omega}_k$, $\hat{\zeta}_k$ govern the shape of the modulus function over the complex s-domain.

The potential and the kinetic energy of the VEM layer are

$$\begin{aligned}
&\frac{1}{2}\int_0^{L_e} G_v b h_v \gamma^2 \, \mathrm{d}x = \frac{1}{2}\{U^{(e)}\}^{\mathrm{T}} [K_{v\gamma}^{(e)}] \{U^{(e)}\}, \\
&\frac{1}{2}\int_0^{L_e} \rho_v h_v b \left(\frac{\partial u_v}{\partial t}\right)^2 \mathrm{d}x + \frac{1}{2}\int_0^{L_e} \rho_v h_v b \left(\frac{\partial w}{\partial t}\right)^2 \mathrm{d}x \\
&\quad = \frac{1}{2}\{\dot{U}^{(e)}\}^{\mathrm{T}} [M_{vu}^{(e)}]\{\dot{U}^{(e)}\} + \frac{1}{2}\{\dot{U}^{(e)}\}^{\mathrm{T}} [M_{vw}^{(e)}]\{\dot{U}^{(e)}\},
\end{aligned} \tag{11}$$

where

$$K_{v\gamma}^{(e)} = G_v b h_v L \int_0^1 [N_\gamma]^{\mathrm{T}} [N_\gamma] \, \mathrm{d}\xi,$$

$$[M_{vu}^{(e)}] = \rho_v h_v b L_e \int_0^1 [N_v]^{\mathrm{T}} [N_v] \, \mathrm{d}\xi, \quad [M_{vw}^{(e)}] = \rho_v h_v b L_e \int_0^1 [N_w]^{\mathrm{T}} [N_w] \, \mathrm{d}\xi.$$

2.1.2. Euler–Bernouilli beam elements

Each of the two nodes of plain beam elements has 3 d.o.f.: the axial and transverse displacements and a rotation. The stiffness and mass matrices of the normal beam elements hence have a dimension of 6×6. The formulation of the matrices is similar to Eqs. (6).

2.1.3. Load vector

If a virtual displacement field is applied on the beam, the virtual work done by an external disturbance force is

$$\delta w_d = \int_0^{L_e} f_d(x,t) \partial w(x,t) \, \mathrm{d}x = [\delta U^{(e)}]^{\mathrm{T}} \{f_d\}. \tag{12}$$

2.1.4. Dynamic equations of a cantilever beam with an ACLD layer

Application of the principle of virtual work and using the above-derived expressions for the potential and kinetic energies lead to the element equilibrium equation. For the ACLD elements, the dynamic equilibrium equations can be written as

$$[M^{(e)}]\{\ddot{U}^{(e)}\} + [K_E^{(e)}]\{U^{(e)}\} + [K_{v\gamma}^{(e)}]\{U^{(e)}\} = \{f_c^{(e)}\}, \tag{13}$$

where

$$[M^{(e)}] = [M_{bu}^{(e)}] + [M_{bw}^{(e)}] + [M_{cu}^{(e)}] + [M_{cw}^{(e)}] + [M_{vu}^{(e)}] + [M_{vw}^{(e)}],$$

$$[K_E^{(e)}] = [K_{bu}^{(e)}] + [K_{bw}^{(e)}] + [K_{cu}^{(e)}] + [K_{cw}^{(e)}].$$

Eq. (13) is non-linear because G_v in $[K_{v\gamma}^{(e)}]$ is not a constant. In Laplace domain the initial conditions have been assumed to be zero, so a column matrix of dissipation co-ordinates are introduced [19]:

$$\{\hat{Z}_k(s)\} = \frac{\hat{\omega}_k^2}{s^2 + 2\hat{\xi}_k\hat{\omega}_k s + \hat{\omega}_k^2}\{U^{(e)}(s)\}. \tag{14}$$

Because a GHM model is used for the VEM, Eq. (13) can now be written as follows:

$$[\bar{M}^{(e)}]\{\ddot{q}^{(e)}\} + [\bar{D}^{(e)}]\{\dot{q}^{(e)}\} + [\bar{K}^{(e)}]\{q^{(e)}\} = \{\bar{f}(e)\}, \tag{15}$$

where

$$\bar{M}^{(e)} = \begin{bmatrix} M^{(e)} & 0 & \cdots & 0 \\ 0 & \alpha_1 \dfrac{1}{\hat{\omega}_1^2}\Lambda & 0 & \vdots \\ \vdots & 0 & \ddots & 0 \\ 0 & \cdots & 0 & \alpha_N \dfrac{1}{\hat{\omega}_N^2}\Lambda \end{bmatrix}, \quad \bar{D}^{(e)} = \begin{bmatrix} 0 & 0 & \cdots & 0 \\ 0 & \alpha_1 \dfrac{2\hat{\xi}_1}{\hat{\omega}_1}\Lambda & 0 & \vdots \\ \vdots & 0 & \ddots & 0 \\ 0 & \cdots & 0 & \alpha_N \dfrac{2\hat{\xi}_N}{\hat{\omega}_N}\Lambda \end{bmatrix},$$

$$\bar{K}^{(e)} = \begin{bmatrix} K_E^{(e)} + K_{v\gamma}^{(e)}(1 + \sum_{k=1}^{N}\alpha_k) & -\alpha_1 R & \cdots & -\alpha_N R \\ -\alpha_1 R^{\mathrm{T}} & \alpha_1\Lambda & 0 & 0 \\ \vdots & 0 & \ddots & 0 \\ -\alpha_N R^{\mathrm{T}} & 0 & 0 & \alpha_N\Lambda \end{bmatrix}, \quad \{q^{(e)}\} = \begin{Bmatrix} U^{(e)} \\ Z_1 \\ \vdots \\ Z_N \end{Bmatrix}, \quad \{\bar{f}^{(e)}\} = \begin{Bmatrix} f_c^{(e)} \\ 0 \\ \vdots \\ 0 \end{Bmatrix},$$

$Z_k = R_v^{\mathrm{T}}\hat{Z}_k$, $R = R_v\Lambda$, $\Lambda = G^{\infty}\Lambda_v$, $[K_{v\gamma}^{(e)}] = G^{\infty}[\hat{K}_{v\gamma}^{(e)}]$, $[\hat{K}_{v\gamma}^{(e)}] = R_v\Lambda_v R_v^{\mathrm{T}}$, Λ_v is a diagonal matrix of the non-zero (necessarily positive) eigenvalues of matrix $\hat{K}_{v\gamma}^{(e)}$, and the corresponding orthonormalized eigenvectors form the columns of the matrix R_v.

Eq. (15) is a traditional second-order form. For the cantilever beam with an ACLD layer, the following global dynamic equation can be derived through standard FEM assembly procedures:

$$[M]\{\ddot{q}\} + [D]\{\dot{q}\} + [K]\{q\} = [F]. \tag{16}$$

2.2. Model reduction process

The dynamic equation (16) derived has an excess of d.o.f.'s from a control point of view. Moreover, it is unobservable and uncontrollable [30,31]. Model reduction is required.

Model reduction methods are developed from two different disciplines [32]: finite element (FE) analysis [33,34] and large-system control theories [30,35]. The former could reduce system size, but it could not guarantee observability and controllability because the model reduction takes place entirely in the physical space. Observability and controllability are thus beyond consideration. The latter could guarantee observability and controllability, but unsuitable for flexile structures like a beam with an ACLD layer. The FE model of the ACLD system has too many d.o.f.'s for adequate control, especially after the introduction of dissipation co-ordinates in Eqs. (14) and (15). What is more, this large system is uncontrollable and unobservable. It is impossible to directly compute the full orthogonal bases for the eigenspace required in intermediate steps in the state space, even by Schur decomposition [34].

A new model reduction procedure is proposed. An iterative dynamic condensation is performed in the physical space, and Guyan condensation is taken as an initial iteration approximation. This results in a reduced order system of suitable size, but still unobservable and uncontrollable. A robust model reduction method is employed in the state space afterwards. Now the system size is reduced, and stability, controllability and observability of the reduced order model (ROM) are assured.

To study observability and controllability of the proposed model reduction procedure conveniently, controllability gramian W_c and the observability gramian W_o are introduced.

Given the continuous-time state-space model

$$\begin{aligned} \dot{x} &= Ax + Bu, \\ y &= Cx + Du, \end{aligned} \tag{17}$$

W_c and W_o are defined by

$$W_c = \int_0^\infty \mathrm{e}^{A\tau} BB^{\mathrm{T}} \mathrm{e}^{A^{\mathrm{T}}\tau}\,\mathrm{d}\tau, \quad W_o = \int_0^\infty \mathrm{e}^{A^{\mathrm{T}}\tau} C^{\mathrm{T}} C \mathrm{e}^{A\tau}\,\mathrm{d}\tau, \tag{18}$$

W_c and W_o can be obtained by solving Lyapunove equations

$$AW_c + W_c A^{\mathrm{T}} + BB^{\mathrm{T}} = 0, \quad A^{\mathrm{T}} W_o + W_o A + C^{\mathrm{T}} C = 0. \tag{19}$$

The system is controllable if W_c is full rank; it is observable if W_o is full rank [32]. The numerical condition of W_c and W_o is a measure of system's controllability and observability.

2.2.1. Model reduction in the physical space

The total number of d.o.f.'s in Eq. (16) is assumed to be n. It can be divided into master d.o.f.'s (the conserved d.o.f.'s) and slave d.o.f.'s (the removed d.o.f.'s). Eq. (16) can be written as

$$\begin{bmatrix} M_{mm} & M_{ms} \\ M_{sm} & M_{ss} \end{bmatrix} \begin{Bmatrix} \ddot{X}_m(t) \\ \ddot{X}_s(t) \end{Bmatrix} + \begin{bmatrix} D_{mm} & D_{ms} \\ D_{sm} & D_{ss} \end{bmatrix} \begin{Bmatrix} \dot{X}_m(t) \\ \dot{X}_s(t) \end{Bmatrix} + \begin{bmatrix} K_{mm} & K_{ms} \\ K_{sm} & K_{ss} \end{bmatrix} \begin{Bmatrix} X_m(t) \\ X_s(t) \end{Bmatrix} = \begin{bmatrix} F_m(t) \\ F_s(t) \end{bmatrix}. \tag{20}$$

If a system reduction matrix $R \in R^{s\times m}$ is defined, which relates the master d.o.f.'s with the slave d.o.f.'s, then after i iterations, the reduced-order system equation [36] is

$$M_R^{(i)}\ddot{X}_m(t) + D_R^{(i)}\dot{X}_m(t) + K_R^{(i)}X_m(t) = F_R^{(i)}(t), \tag{21}$$

where

$$M_R^{(i)} = M_{mm} + (R^{(i)})^{\mathrm{T}}M_{sm} + M_{ms}R^{(i)} + (R^{(i)})^{\mathrm{T}}M_{ss}R^{(i)},$$

$$D_R^{(i)} = D_{mm} + (R^{(i)})^{\mathrm{T}}D_{sm} + D_{ms}R^{(i)} + (R^{(i)})^{\mathrm{T}}D_{ss}R^{(i)},$$

$$K_R^{(i)} = K_{mm} + (R^{(i)})^{\mathrm{T}}K_{sm} + K_{ms}R^{(i)} + (R^{(i)})^{\mathrm{T}}K_{ss}R^{(i)}, \quad F_R^{(i)}(t) = F_m(t) + (R^{(i)})^{\mathrm{T}}F_s,$$

$$R^{(i+1)} = -K_{ss}^{-1}[M_{ss}R^{(i)}(M_R^{(i)})^{-1}K_R^{(i)} - K_{sm}].$$

Guyan [33] condensation is taken as an initial iteration approximation. So $R^{(0)} = -K_{ss}^{-1}K_{sm}$.

In this reduction, two issues must be addressed: selection of the master d.o.f.'s and their number. Levy [37] gave guidance on choosing master d.o.f.'s. He recommended the choice of d.o.f.'s with large displacements in the useful band or large mass components. Ramsden and Stocker [38] selected the master d.o.f.'s associated with large mass concentrations and those reasonably flexible with respect to other mass concentrations. Downs [39] insisted master d.o.f.'s must be translations instead of rotations. In complicated assemblies, master d.o.f.'s were to be found in the most flexible regions. Shah and Raymund [40] proposed an eliminated algorithm, such that the ratio k_{ii}/m_{ii} of the diagonal terms of K and M corresponding to the removed slave d.o.f.'s is a maximum. The number of interested modals determines the number of master d.o.f.'s. Levy [37] advised that the ratio between the number of the master d.o.f.'s and the number of the interested modals should be 3.5. Ramsden and Stocker [38] thought that the ratio should be a value between 2 and 3. Suarez and Singh [41] proposed a 1.40 ratio. Those conflicting theories make it difficult to resolve the issue of master d.o.f.'s selection and their number. Different problems will require different solutions.

2.2.2. *Model reduction in the state space*

The reduced-order system equation (21) is much smaller than the original system equation (16), but it is unobservable and uncontrollable in the state space. A robust model reduction follows in the state space. Generally speaking, the robust model reduction method has the following special features: (1) It bypasses the ill-conditioned balanced transformation. (2) It employs Schur decomposition to compute robustly the orthogonal bases for eigenspace required in intermediate steps. (3) It has a H^{∞}-norm error bound. The infinity norm of the relative error or the absolute error of the ROM is bounded by a precomputable positive real number for all frequencies.

Eq. (21) can be transformed into the state-space form (A, B, C, D) with $2m$ d.o.f.'s. Its transfer function is $G(s) = D + C(Is - A)^{-1}B$. It can be reduced to a system $(\hat{A}, \hat{B}, \hat{C}, \hat{D})$ with k $(k<2m)$ d.o.f.'s. The detailed procedure can be found in Ref. [30].

2.3. Controller design

For the final ROM $(\hat{A}, \hat{B}, \hat{C}, \hat{D})$, the linear-quadratic-Gaussian (LQG) controller [36] is

$$\dot{\hat{x}} = [\hat{A} - \hat{B}K - L\hat{C} + L\hat{D}K]\hat{x} + Ly, \quad \hat{u} = -K\hat{x}, \tag{22}$$

where $K = R^{-1}\hat{B}^{\mathrm{T}}P$, $L = P_0\hat{C}^{\mathrm{T}}R_0^{-1}$, P and P_0 can be solved from the following two Riccati equations:

$$\hat{A}^{\mathrm{T}}P + P\hat{A} - P\hat{B}R^{-1}\hat{B}^{\mathrm{T}}P + Q = 0, \quad \hat{A}^{\mathrm{T}}P_0 + P_0\hat{A} - P_0\hat{C}^{\mathrm{T}}R_0^{-1}CP_0 + FQ_0F^{\mathrm{T}} = 0, \tag{23}$$

where P is the semi-positive-definite weighting matrices on the states, Q is the positive-definite weighting matrices on the control inputs. P_0 and Q_0 are the input noise intensity and measurement noise intensity. Vector F denotes the disturbance position. y is the measurable output of the system $(\hat{A}, \hat{B}, \hat{C}, \hat{D})$.

3. Numerical simulation and experimental study

In this section, the numerical simulation of a real cantilever beam with an ACLD layer is performed based on the above analysis, next modal experiments are used to verify the simulation. Finally a real-time control system is designed based on the verified model.

3.1. Numerical simulation

The dimensions of the real cantilever beam with an ACLD layer in Fig. 1 are listed in Table 1. The PZT and VEM are provided separately by Haiying corporation in Wuxi, China, and the institute of aerospace technology in Beijing, China. The disturbance is exerted at the free tip of the cantilever beam; the transverse displacement responses are measured there as well.

3.1.1. FEM analysis

In Fig. 1, the left part of plain beam (LL) is divided into 3 normal Euler–Bernouilli beam elements, the right part (LR) into 6 and the middle part into 6 ACLD elements. The modal frequencies (Hz) and damping ratios of the first four modes are given in Table 2.

The modal experiment will be discussed in more detail later. From Table 2, the following conclusion can be drawn: (1) The frequencies calculated with FE model agree well with those from experiments. It shows that the mathematical model derived by FEM is accurate enough for designing a controller. (2) The frequencies from FEM are only a little bit higher than those

Table 1
System parameters

L	0.400 m	h_b	0.003 m	E_b	5×10^{10} N/m^2	α_2	4.1977×10^1	$\hat{\xi}_1$	3.0787
LL	0.093 m	h_v	0.001 m	E_c	6.67×10^{10} N/m^2	α_3	3.5174×10^1	$\hat{\xi}_2$	1.4288×10^2
LR	0.202 m	ρ_c	7450 kg/m^3	d_{31}	-1.85×10^{-10} m/V	$\hat{\omega}_1$	6.6169×10^6	$\hat{\xi}_3$	6.1785×10^2
b	0.014 m	ρ_v	789.5 kg/m^3	G^{∞}	3.8870×10^4 Pa	$\hat{\omega}_2$	3.2854×10^4		
h_c	0.0007 m	ρ_b	2700 kg/m^3	α_1	2.3263×10^4	$\hat{\omega}_3$	4.7515×10^4		

Table 2
FEM and modal experimental results

Mode	FEM results	Experimental results	Relative errors (%)
f_1	13.0118 Hz	12.71 Hz	2.3745
η_1	1.6772%	1.52%	10.3421
f_2	73.7874 Hz	73.64 Hz	0.20016
η_2	1.1527%	1.41%	18.2482
f_3	212.2858 Hz	211.43 Hz	0.4048
η_3	1.6479%	1.61%	2.3540
f_4	415.6184 Hz	413.16 Hz	0.5950
η_4	0.9234%	0.82%	12.6098

Table 3
The first 4 frequencies of EM, FOM and ROM

Mode	EM (Hz)	FOM (Hz)	ROM (Hz)	Relative errors (%)
1	12.71	13.0118	13.0162	0.03382
2	73.64	73.7874	73.9063	0.1610
3	211.43	212.2858	214.1771	0.8909
4	413.16	415.6184	437.2304	5.199

obtained from experiments, this is reasonable. (3) The difference between damping ratios from FEM and those from experiments is somewhat bigger, but remains acceptable (damping ratios cannot be measured accurately).

3.1.2. Model reduction

The above system derived by FEM has 106 d.o.f.'s in the physical space and 212 d.o.f.'s in the state space. The system has too many degrees for control design. Furthermore, it is unobservable and uncontrollable. It is necessary to perform model reduction and make the system observable and controllable before a controller can be designed.

According to Section 2.2.1, 8 transverse displacements of the 9 Euler–Bernouilli beam elements, 7 transverse displacements of base beam layer, 7 transverse and 7 axial displacements of the PZT layer in the 6 ACLD elements are chosen as master d.o.f.'s. All other d.o.f.'s including the dissipation d.o.f.'s resulted from GHM model, the rotations and axial displacements of base beam become slave d.o.f.'s. By using Eqs. (20) and (21), the system is reduced from 106 d.o.f.'s to 29 d.o.f.'s in the physical space. By using the procedure mentioned in Section 2.2.2, the system is further reduced from 58 d.o.f.'s to 11 d.o.f.'s in the state space.

The final ROM becomes 11×11 in the state space after the model reduction firstly in the physical space and then in the state space. The first 4 frequencies of experimental model (EM), the original full order model (FOM) and ROM are listed in Table 3. The relative errors are taken between FOM and ROM. According to Section 2, the conditions of W_c and W_o are good measure

of controllability and observability. The conditions of W_c and W_o of the FOM and ROM are listed in Table 4.

It can be seen from Table 3 that (1) the final ROM agrees well with the original FOM in low-frequency range. The relative errors of the first three modes between FOM and ROM are less than 1%; (2) the frequencies of FOM are smaller than those of ROM; (3) the relative errors increase with the mode number.

It can be seen from Table 4 that (1) the final ROM is far smaller than the original FOM; (2) the ROM is both controllable and observable.

When a voltage is applied to the PZT, the Bode graph between the PZT layer and the free tip of the cantilever beam is shown in Fig. 3. When a disturbance is exerted at the free tip of the cantilever beam, the Bode graph is shown in Fig. 4.

It is shown in Figs. 3 and 4 that the final ROM agrees well with the original FOM in low-frequency range.

When a unit impulse voltage is exerted on the PZT, the transverse displacement response at the free tip of the cantilever beam is shown in Fig. 5. When a unit impulse disturbance is exerted at the free tip of the cantilever beam, the transverse displacement response is shown in Fig. 6.

Table 4
The condition of W_c and W_o of the FOM and the FROM

	Size (W_c)	Rank (W_c)	Size (W_o)	Rank (W_o)
FOM	212	84	212	78
ROM	11	11	11	11

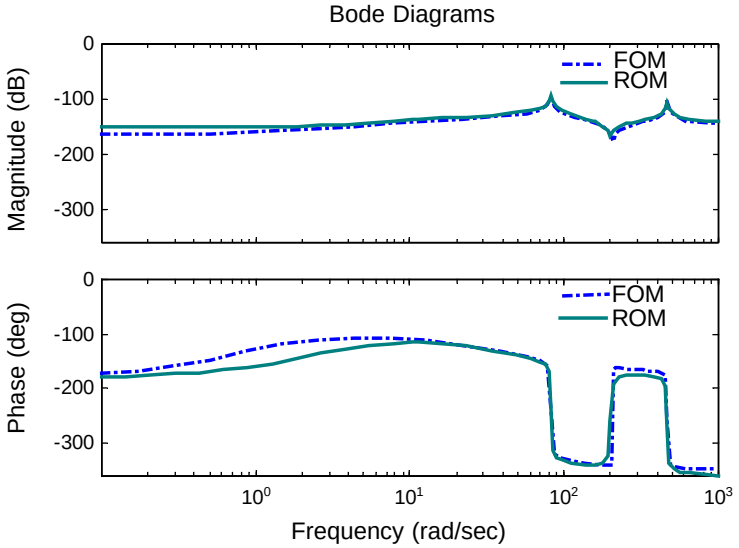

Fig. 3. Bode graph between the PZT layer and the free tip of the cantilever beam (applied voltage).

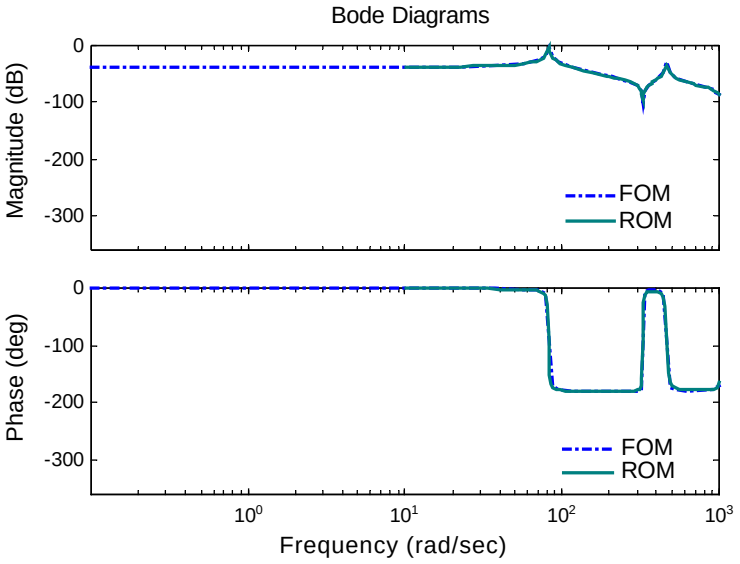

Fig. 4. Bode graph between the PZT layer and the free tip of the cantilever beam (disturbance force).

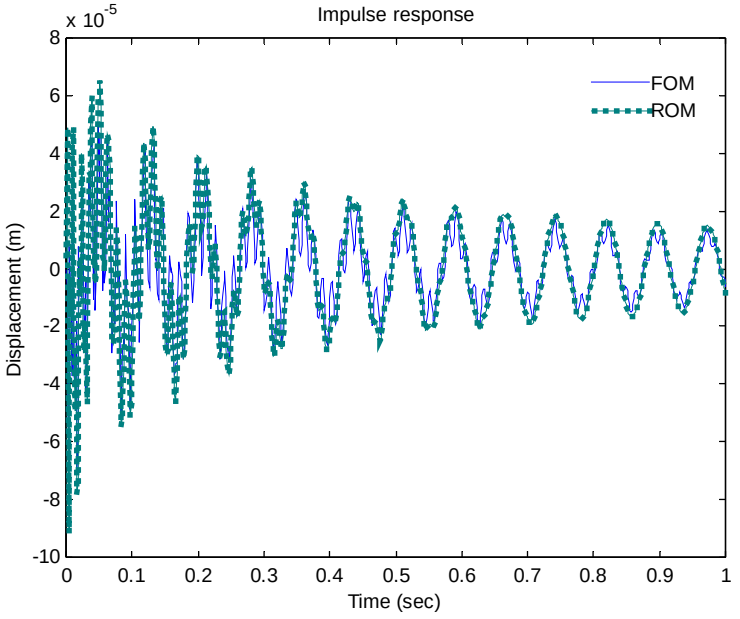

Fig. 5. Transverse displacement response for a unit impulse voltage.

3.1.3. Controller design

The controllable and observable ROM obtained in above section accurately represents the FOM of the ACLD system. A ROM-based controller is designed according Section 2.3. When a

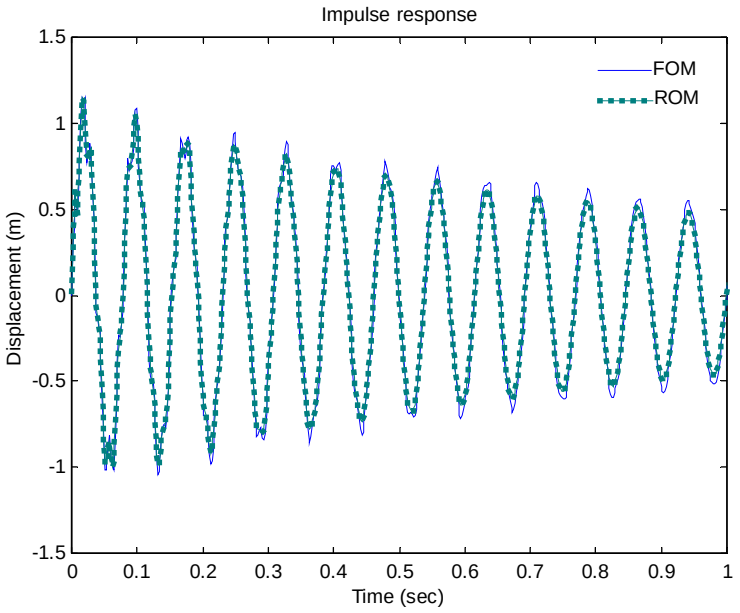

Fig. 6. Transverse displacement response for a unit impulse disturbance.

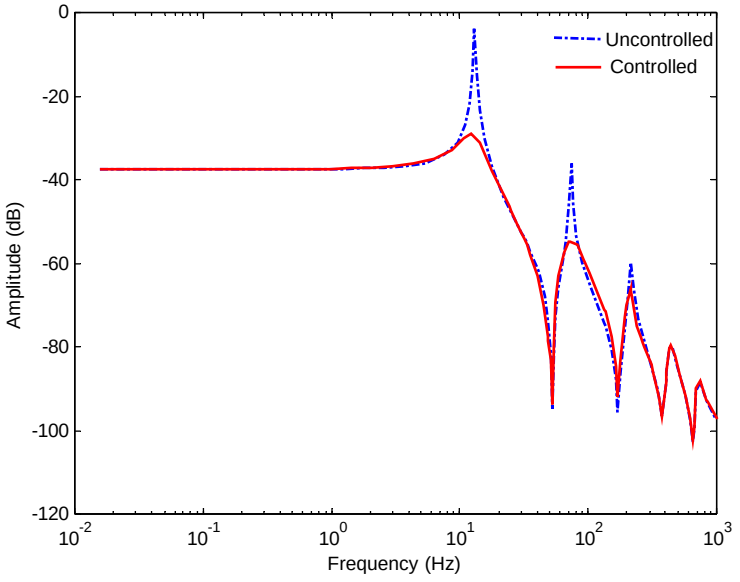

Fig. 7. Controlled and uncontrolled frequency response functions.

disturbance is exerted at the free tip of the cantilever beam and a control voltage is applied to PZT, the frequency response function (FRF) is shown in Fig. 7.

It is shown in Fig. 7 that the control effect is obvious in low-frequency range, especially for the first 2 modes.

The above controller is 11×11 in the state space. The model reduction of the above controller is also performed because if the controller small then during the course of real-time control it is better. The controller is reduced to 6×6 by using the procedure mentioned in Section 2.2.2. The input of the controller is the output of the system, namely the sensor, while the output of the controller is the input of the system, namely the actuator. Its Bode graph is shown in Fig. 8. It is clear that the performance of the controller is not reduced after model reduction.

3.2. Experimental study

In Section 3.1, a 11×11 ROM and a 6×6 reduced controller are prepared. In this section, modal analysis is performed to verify the FEM model and a real-time control system is set to test the control effect.

3.2.1. Experimental modal analysis

The experimental setup for the modal analysis is shown in Fig. 9. E1 is the force sensor at the excited point. S1–S5 are 5 PCB acceleration sensors. Other instruments include 1 HP35605 analyzer, 1 CADA-X workstation, 1 B&K 900803 charge amplifier and 5 PCB charge amplifiers.

The FRF between E1 and S5 is shown in Fig. 10. The first 4 modal frequencies are listed in Table 3. It is shown in Fig. 10 and Table 3 that the mathematical model derived by FEM is accurate enough to design a suitable controller for the experimental cantilever beam.

3.2.2. Real-time active control study

In Section 3.1.3, a reduced 6×6 controller is derived. The weighting matrices Q and R are $5 \times 10^6 \times \mathrm{I}$ and 1×10^{-4}, respectively, I is the unit matrix with suitable size. The input noise intensity Q_0 and the measurement noise intensity R_0 are 1×10^{-3} and 1×10^{-10}, respectively. It can be transformed to a discrete form which is suitable to a PC real-time control system. The

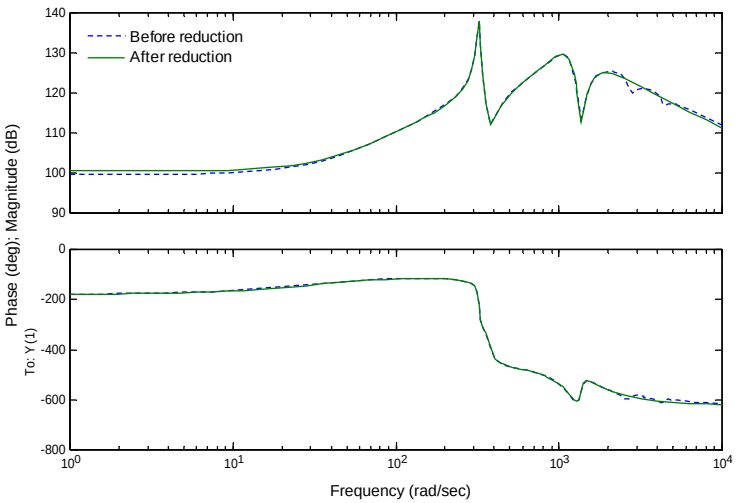

Fig. 8. A Bode graph of the controller before and after model reduction.

experimental setup for the real-time control study is shown in Fig. 11. The main instruments include a IPC5472 A/D & D/A card, a PC, a NH-Z 600 power amplifier, a non-contact current vortex sensor (CVS) at the free tip of the cantilever beam, and a weight suspended at the free tip of the cantilever beam by a very light, thin cord.

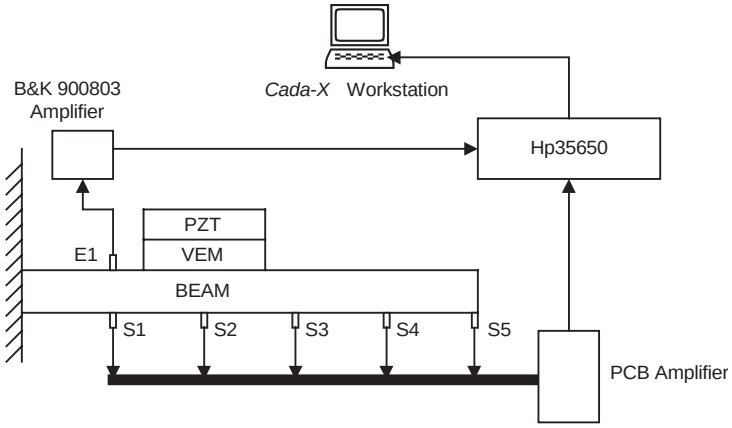

Fig. 9. Experimental setup for the modal analysis.

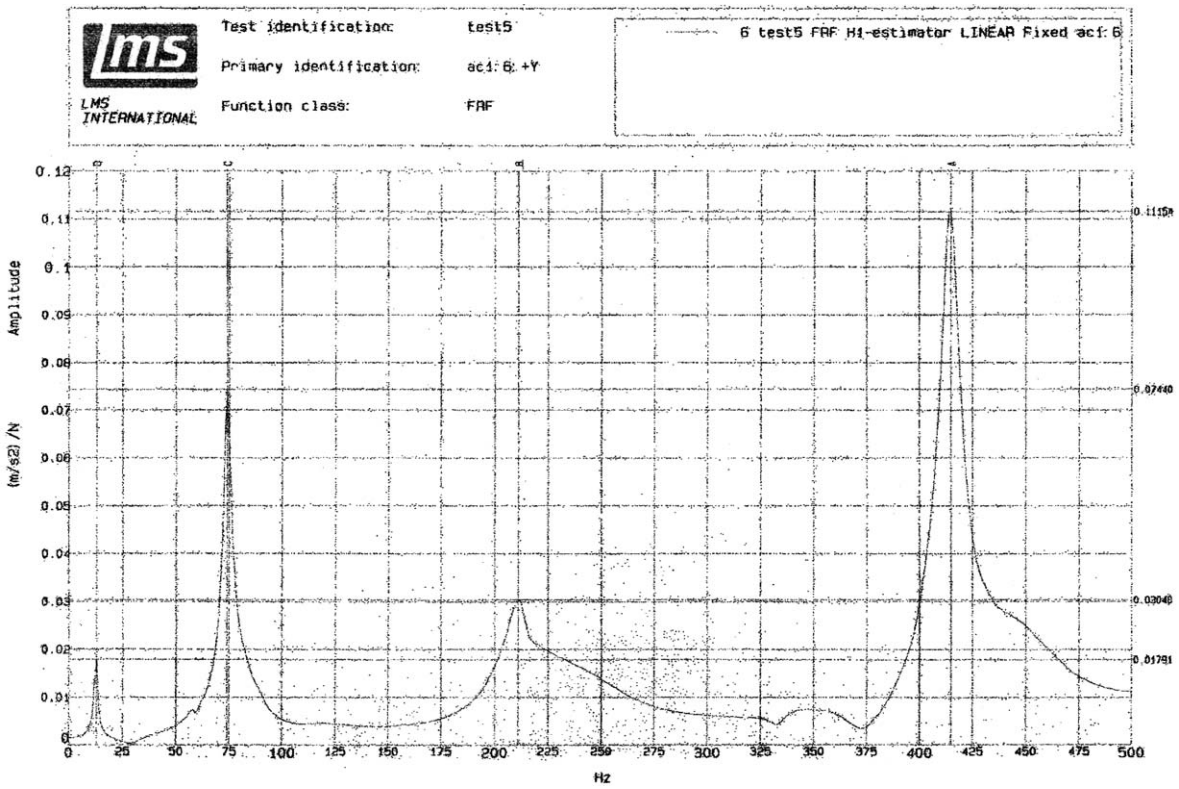

Fig. 10. The FRF between E1 and S5.

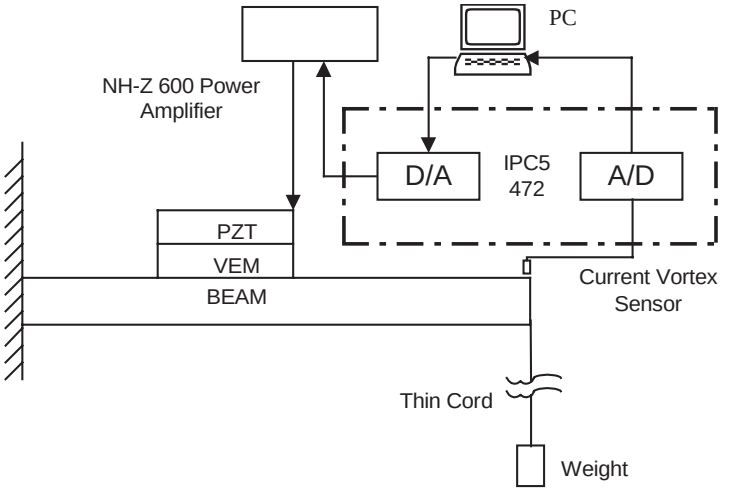

Fig. 11. Experimental setup for real-time control study.

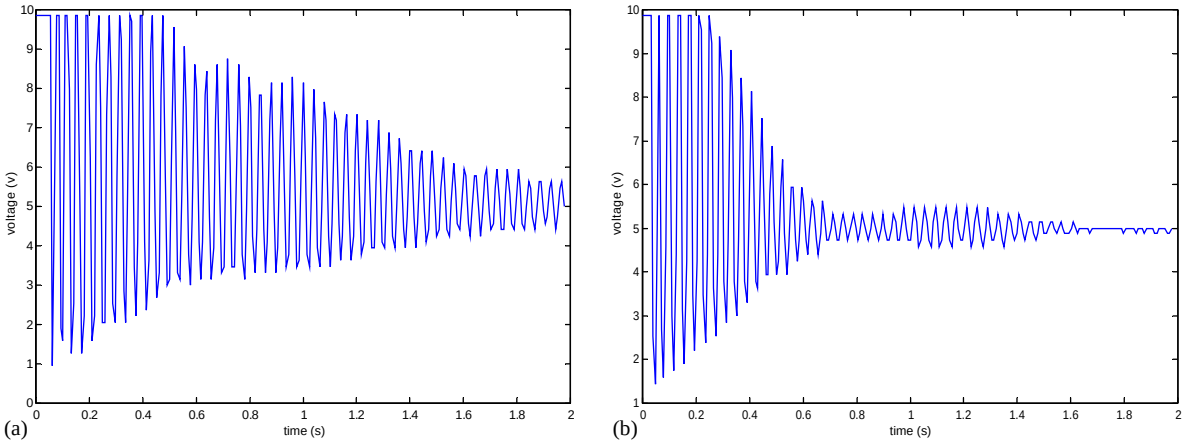

Fig. 12. The measured impulse response (in voltage) of the (a) uncontrolled system, (b) controlled system.

In this real-time control experiment, the transverse displacement at the free tip of the cantilever beam is measured by the CVS. The weight is suspended at the free tip of the cantilever beam by a very light, thin cord. The cord is cut suddenly. This is used to simulate an impulse disturbance at the free tip. A voltage output from the controller is applied to the PZT to attenuate the vibration. This procedure was repeated many times, always yielding similar results.

A typical measured transverse displacement response at the free tip of the uncontrolled cantilever beam is shown in Fig. 12(a). The corresponding controlled responses is shown in Fig. 12(b). From this pair of figures, it is obvious that the impulse responses are attenuated after the control voltage computed by the designed controller is applied to the PZT.

The responses in Figs. 12(a) and (b) are transformed into the frequency domain by a FFT. The corresponding power spectral density (PSD) is shown in Fig. 13. It clearly shows that the first 2 frequencies are attenuated. The PSD at the first frequency is reduced from 248.0656 to 61.0946.

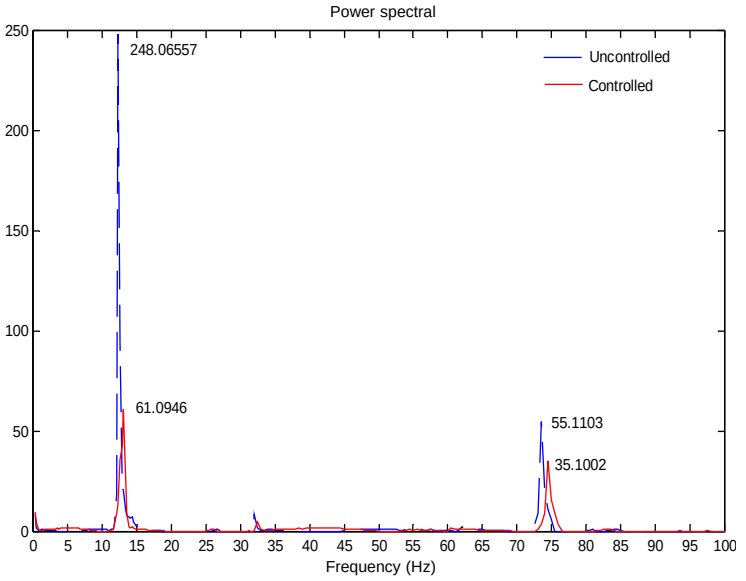

Fig. 13. The power spectral density of the controlled and uncontrolled system.

The controlled PSD at the first frequency is 24.6284% of the uncontrolled. The PSD at the second frequency is reduced from 55.1103 to 35.1002. The controlled PSD at the second frequency is 63.6908% of the uncontrolled.

4. Conclusion

It has been shown in this paper that it is possible to overcome vibration control problems due to model size and lack of controllability and observability. The proposed method first derives a finite element model of a structure with hybrid damping treatment and next uses a reduction method to obtain a small size, controllable and observable model. It has been shown that it is possible to design a controller based on the reduced model.

Finally, experimental validation by a real-time control system was set up. The controlled and uncontrolled impulse responses at the free tip of the cantilever beam with ACLD treatment were compared both in time domain and frequency domain. The results have clearly shown the effect of the control.

The procedure proposed in this paper can, in principle, be applied to other more complex structures. Future research will go in this direction.

Acknowledgements

This work is part of a project supported by the foundation of the National Science and Technology Key Laboratory under the project number JS 52.4.3. This support is gratefully acknowledged.

Appendix. Nomenclature

b	width of the ACLD beam
D	electrical displacement
d_{31}	piezoelectric constant
$[D]$	damping matrix
$E_{c,b}$	Young's modulus of the PZT layer and the base beam, respectively
E	electrical field
$[F]$	general force including the effect of external disturbances and the PZT layer
$f_c^{(e)}$	general force of the PZT layer
$f_d^{(e)}$	general force of external disturbances
G^{∞}	equilibrium value of the shear modulus
G_v	shear modulus of the VEM in the time domain
$h_{c,v,b}$	thickness of the PZT layer, the VEM layer and the base beam, respectively
$I_{c,b}$	moment of inertia of the PZT layer and the base beam, respectively
$[K]$	stiffness matrix
L_e	length of the ACLD elements
L	length of the ACLD part
LL	length of the left part of the ACLD beam
LR	length of the right part of the ACLD beam
$[M]$	mass matrix
$N_{w,c,b,v,r}$	shape function of the transverse displacement, the axial displacement of the PZT layer, the axial displacement of the base beam, the axial displacement of the VEM layer, and the shear strain of the VEM layer, respectively
S_{11}^E	elastic compliance constant
$s\bar{G}(S)$	complex modulus of the VEM layer
$U^{(e)}$	local nodal displacement column
$u_{c,b}$	axial displacement of the PZT layer and the base beam, respectively
$V(t)$	applied voltage on the PZT layer
w	transverse displacement
$\hat{z}_k(s)$	dissipation co-ordination
$\alpha_k, \hat{\omega}_k, \hat{\zeta}_k$	positive constants of the GHM model
γ	shear strain of the VEM layer
ε	mechanical strain in the axial direction
ε_{33}^{τ}	dielectric constant
θ	rotation angle
$\rho_{c,v,b}$	density of the PZT layer, the VEM layer and the base beam, respectively
σ_i	Hankel singular values of the system
τ	mechanical stress in the axial direction

Superscript

$'$	partial differentiation with respect to x

Subscripts

b	index for the base beam

c	index for the PZT constraining layer
i, j	index for the element nodes i,j
m	index for master d.o.f.'s
s	index for the slave d.o.f.'s
R	index for the reduced order system
u	axial displacement
v	viscoelastic layer
w	transverse displacement
γ	shear strain of VEM layer

References

[1] B.C. Nakra, Vibration control with viscoelastic material III, *Shock and Vibration Digest* 16 (1984) 17–22.
[2] A.K. Lall, N.T. Asnani, B.C. Nakra, Damping analysis of partially covered sandwich beams, *Journal of Sound and Vibration* 123 (1988) 247–259.
[3] A. Bhimaraddi, Sandwich beam theory and the analysis of constrained layer damping, *Journal of Sound and Vibration* 179 (1995) 591–602.
[4] F.E. Crawly, J.D. Luis, Use of piezoelectric actuators as element of intelligent structures, *American Institute of Aeronautics and Astronautics Journal* 25 (1987) 1373–1385.
[5] T. Baily, J.E. Hubbard, Distributed piezoelectric polymer active vibration control of a cantilever beam, *Journal of Guidance, Control and Dynamics* 8 (1985) 605–611.
[6] S.S. Rao, T.S. Pan, Optimal placement of actuators in actively controlled structures using genetic algorithms, *American Institute of Aeronautics and Astronautics Journal* 29 (1991) 442–443.
[7] A. Baz, J. Ro, The concept and performance of active constrained layer damping treatments, *Sound and Vibration* 3 (1996) 18–21.
[8] S. Shimamura, A concept of intelligent materials, *Bulletin of the Japan Institute of Metals* 23 (1984) 656–661.
[9] J.A. Rongong, J.R. Wright, Modeling of a hybrid constrained layer/Piezoceramic approach to active damping, *Journal of Vibration and Acoustic* 119 (1) (1997) 120–130.
[10] A. Baz, Optimization of energy dissipation characteristics of active constrained layer damping, *Journal of Smart Material and Structures* 6 (1997) 360–368.
[11] I.Y. Shen, Hybrid damping through intelligent constrained layer treatments, *American Society of Mechanical Engineers, Journal of Vibration and Acoustics* 116 (1994a) 341–349.
[12] A. Baz, J. Ro, Vibration control of plate with active constrained layer damping, *Journal of Smart Materials and Structures* 5 (1996) 272–280.
[13] Qian Chen, The Dynamic Analysis of Viscoelastic Compound Structures, Ph.D. Dissertation, College of Nanjing Aviation, Nanjing, China.
[14] D.E. Veley, S.S. Rao, A comparison of active, passive and hybrid damping in structural design, *Journal of Smart Materials and Structure* 5 (1996) 660–671.
[15] S.H. Crandall, The role of damping in vibration theory, *Journal of Sound and Vibration* 11 (1) (1970) 3–18.
[16] G.A. Lesieutre, E. Bianchini, Time domain modeling of linear viscoelasticity using anelastic displacement fields, *Journal of Vibration and Acoustics* 117 (1995) 424–430.
[17] G.A. Lesieutre, U. Lee, A finite element for beams having segmented active constrained layers with frequency-dependent viscoelastics, *Journal of Smart Materials and Structures* 5 (1996) 615–627.
[18] D.J. McTavish, P.C. Hughes, Finite element method of linear viscoelastic structures: the GHM method, *AIAA-92-2380*, 1992.
[19] D.J. McTavish, P.C. Hughes, Modeling of linear viscoelastic space structures, *American Society of Mechanical Engineers, Journal of Vibration and Acoustics* 115 (1993) 103–133.

[20] J.L. Margaretha, Vibration control through passive constrained layer damping and active control, *Journal of Intelligent Material Systems and Structures* 8 (1997) 663–677.
[21] W.H. Liao, K.W. Wang, On the active-passive hybrid control actions of structures with active constrained layer treatments, *Journal of Vibration and Acoustics* 119 (1997) 563–572.
[22] W.H. Liao, K.W. Wang, On the analysis of viscoelastic material for active constrained layer damping treatments, *Journal of Sound and Vibration* 207 (3) (1997) 319–334.
[23] Y. Shi, The modeling and vibration control of beams with active constrained layer damping, *Journal of Sound and Vibration* 245 (5) (2001) 785–800.
[24] A. Baz, Boundary control of beams using active constrained layer damping, *Journal of Vibration and Acoustic* 119 (1997) 166–172.
[25] A. Baz, Robust control of active constrained layer damping, *Journal of Sound and Vibration* 211 (3) (1998) 467–480.
[26] W.C. Van Nostrand, Finite element methods for active constrained layer damping, *Passive Damping, North American Conference on Smart Structures and Materials*, Orlando, FL, 1994, pp. 126–137.
[27] M.I. Friswell, D.J. Inman, Finite element models with viscoelastic damping, *Proceedings of IMAC XVII*, Kissimmee, FL, 1999, pp. 181–187.
[28] M.W. Zehn, M. Enzmann, Simulation of structure control and controller design within a finite element code, *Journal of Vibration and Control* 6 (2) (2000) 223–242.
[29] D.J. Mead, S. Markus, The forced vibration of a three-layer damped sandwich beam with arbitrary boundary conditions, *Journal of Sound and Vibration* 10 (1969) 163–175.
[30] M.G. Safonov, R.Y. Chiang, A Schur method for balanced-truncation model reduction, *IEEE Transaction on Automatic Control* 34 (1989) 687–695.
[31] M. Athans, The role and use of the stochastic linear-quadratic-Gaussian problem in control system design, *IEEE Transaction on Automatic Control* AC-16, 1971, pp. 529–552.
[32] K.H. Yae, D.J. Inman, Control-oriented order reduction of finite element model, *Journal of Dynamic Systems, Measurement, and Control* 115 (1993) 708–711.
[33] R.J. Guyan, Reduction of stiffness and mass matrices, *American Institute of Aeronautics and Astronautics Journal* 3 (1965) 380.
[34] M. Paz, Practical reduction of structural eigenproblems, *Journal of Structural Engineering* 109 (1983) 2591–2599.
[35] E.J. Davision, A method for simplifying linear dynamic systems, *IEEE Transaction on Automatic Control* AC-11, 1996, pp. 93–101.
[36] Z.Q. Qu, A multi-step method for matrices condensation of finite element methods, *Journal of Sound and Vibration* 214 (1998) 965–971.
[37] R. Levy, Guyan reduction solutions recycled for improved accuracy, NASTRAN User Experiences, NASA, 1971, pp. 201–220.
[38] J.N. Ramsden, J.R. Stocker, Mass condensation—a semi-automatic method for reducing the size of vibration problems, *International Journal for Numerical Method in Engineering* 1 (1969) 339–349.
[39] B. Downs, Accurate reduction of stiffness and mass matrices for vibration analysis and a rationale for selecting master degrees of freedom, *American Society of Mechanical Engineers, Journal of Mechanical Design* 102 (2) (1980) 412–416.
[40] V.N. Shah, M. Raymund, Analytical selection of masters for the reduced eigenvalue problem, *International Journal for Numerical Method in Engineering* 18 (1) (1982) 89–98.
[41] L.E. Suarez, M.P. Singh, Dynamical condensation method for structural eigenvalue analysis, *American Institute of Aeronautics and Astronautics Journal* 30 (4) (1992) 1046–1054.